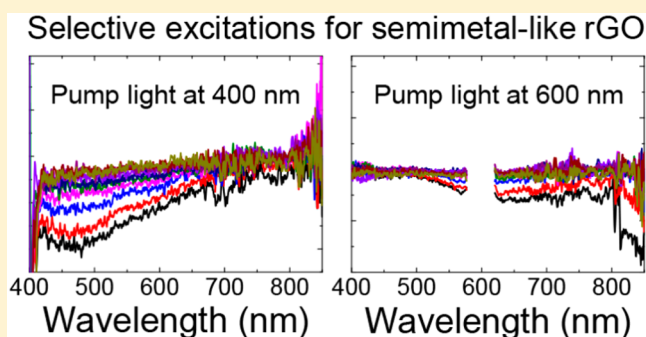


Ultrafast Spectroscopic Study of Insulator–Semiconductor–Semimetal Transitions in Graphene Oxide and Its Reduced Derivatives

Yan Wang,[†] Lei Wang,^{*,†,‡} Hai-Yu Wang,^{*,†} Qi-Dai Chen,^{†,‡} and Hong-Bo Sun^{†,‡}[†]State Key Laboratory of Integrated Optoelectronics, College of Electronic Science and Engineering, Jilin University, 2699 Qianjin Street, Changchun 130012, China[‡]State Key Laboratory of Precision Measurement Technology and Instruments, Department of Precision Instrument, Tsinghua University, Haidian, Beijing 100084, China

S Supporting Information

ABSTRACT: In graphene oxide (GO)-based compound photocatalysts, where GO is a novel cocatalyst, the mainly photophysical processes are the charge separation/transfer between GO and other nanocatalysts. However, the understanding on electronic structures of GO and reduced GO (rGO) is still unclear, despite the fact that it could be one of the most significant keys to improve the photocatalytic performances of GO-based compound photocatalysts. Here, we discuss the relationship of oxygen content of GO and its electronic structure by femtosecond transient absorption spectroscopy and X-ray photoelectron spectroscopy. We find that as-prepared GO and rGO samples with the oxygen content of ~35% are still “insulators”. When the oxygen content slightly decreases to ~34%, the rGO samples begin to exhibit semiconductor-like properties. Moreover, the band gap of those semiconductor-like rGO samples would not continue red shift as further reduction of oxygen content. When the oxygen content of rGO is further reduced to ~29%, rGO begins to possess semimetal-like material characteristic, presenting a two-phase (semiconductor/semimetal) coexistence state due to the nature of inhomogeneity of rGO. Thus, the insulator–semiconductor–semimetal transitions in GO and its reduced derivatives is directly observed in transient spectroscopy, demonstrating that those transitions initially occur in such a relatively narrow range of oxygen content. Especially, for the semimetal-like state of rGO, our findings explain their dual roles in photoelectron conversion (semiconductor part) and electrical transport (semimetal part) applications. It will be helpful for understanding the photophysical properties and related functional information for GO-based optoelectronic devices.



INTRODUCTION

Graphene oxide (GO) and its reduced derivatives have a lot of unique and excellent properties, which has attracted widespread attention in various scientific fields.^{1–5} A large number of oxygen-containing functional groups that are of great significance for GO are randomly distributed on the basal plane and edges of GO.^{6–8} Due to the inhomogeneous arrangement of oxygen-containing functional groups, sp² clusters with high carrier mobility are isolated like a small “island” on the GO sheets. However, if charge transfer cannot occur between different sp² clusters, it should only give rise to the “insulator”-like photoelectric characteristics for GO. In order to enhance the photoelectric properties of GO through connecting more isolated sp² clusters, different methods are used to removing oxygen-containing functional groups and increasing the distribution density of sp² clusters and coverage of sp² areas on the GO sheets.^{9–11} As a result, reduced GO (rGO) samples are created.

As the number of oxygen-containing functional groups decreases, rGO will evolve from an insulator to a semiconductor.¹² Compared with GO, rGO can help to achieve higher performance when GO and rGO are compounded with other nanoparticles forming GO-based nanocomposites, which have been used in photocatalytic and optoelectronic devices.^{13–16} For example, Qu et al. fabricated flexible graphene hydroelectric generators by laser reducing and tailoring GO films.¹⁶ However, it is frustrating that the current understanding on the electronic structures (or band gaps) of GO and rGO is still insufficient, despite the fact that it is an important factor to effectively enhanced the efficiency of those GO-based nanocomposites in photocatalytic and optoelectronic devices.

Received: April 26, 2019

Revised: August 13, 2019

Published: August 21, 2019

To date, the steady-state characterization techniques such as X-ray-based spectroscopies and transmission electron microscopy allow us to realize the atomic structures of GO and rGO, and preliminary understand a part of their electronic structures.^{17–20} It is well-known that there is an assumption that rGO could change from a semiconductor to a semimetal, and this transition is probably related to the number of oxygen-containing functional groups (oxygen content) on rGO sheets, which has been qualitatively reported from the steady-state electrical conduction mechanism point of view,^{21–23} but not been quantitatively investigated in time-resolved spectroscopic experiments yet. So, in order to understand the photophysical properties of GO and rGO more comprehensively, we need to reveal the relationship between electronic structures of GO and rGO and their oxygen contents.

According to our previous reports, broad-band selective excitation transient absorption spectroscopy can be utilized to detect the electronic structure of GO and photothermal-reduced rGO.²⁴ Here, we use the combination of broad-band selective excitation transient absorption spectroscopy and X-ray photoelectron spectroscopy (XPS) to explore the electronic structures of as-prepared GO and rGO with different oxygen contents by controlling the solution–thermal reduction time for each sample (longer reduction time, lower oxygen content in rGO). We have observed the transient spectroscopic changes in the electronic structures of GO and rGO that involve the initial transitions from insulator to semiconductor, and even to a semimetal-like state as the oxygen content of GO and rGO samples decreases in sequence. Moreover, a quantitative analysis of the relationship between the oxygen content and band gap of rGO is presented.

EXPERIMENTAL SECTION

For the femtosecond pump–probe experiments, the output light is at 800 nm wavelength from a mode-locked Ti:sapphire laser/amplifier system (Solstice, Spectra-Physics).^{24–26} It has 1.5 mJ pulse energy with a 100 fs pulse width and a 250 Hz repetition rate. Then, it is split into two parts: one is the excitation light with stronger intensity (the 400 nm excitation light is directly doubled from 800 nm laser pulses; for other desired excitation lights, this beam is used to generate through a TOPAS system), and the other is the probe light (it is tightly focused on a 2 mm thick water to generate supercontinuum white light from 400 to 850 nm). The transient absorption data were collected by a fiber spectrometer. The group velocity dispersion of the transient spectra was compensated by a chirp program. All of the transient experiments were carried out at room temperature.

RESULTS AND DISCUSSION

Steady-State Absorption. We have prepared four GO/rGO samples from sample 1 to sample 4 with the reduction of oxygen content in sequence. As-prepared GO (sample 1) forms a homogeneous brown solution, due to the existence of rich oxygen-containing functional groups, such as $-\text{OH}$, $-\text{COOH}$, and so on. The color of the samples changes from brown in sample 1 to light black in sample 4 with the longest reduction time. Moreover, the solubility of samples is gradually reduced from the sample 1 to sample 4. Typical UV–vis absorption spectra of GO and rGO samples are shown in Figure 1. It confirms that the absorption values of sample 4 in the whole detection range are lower than that of sample 1,

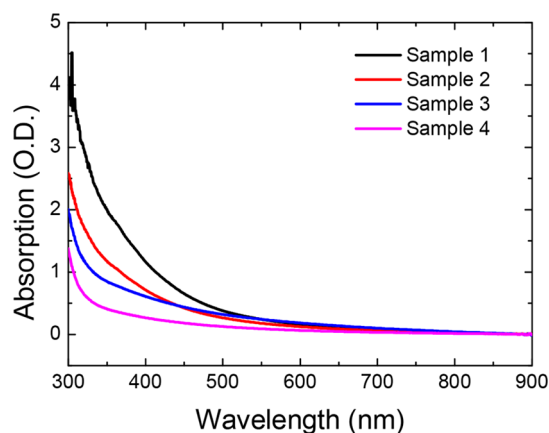


Figure 1. Typical steady-state absorption spectra of GO (sample 1) and rGO (sample 2 to sample 4) samples.

because of the lower solubility for rGO. Interestingly, the contribution of light scattering to the steady-state absorption spectra for all the rGO samples is minimal in the detection range from around 550–850 nm, after carefully comparing the steady-state absorption spectra with transient absorption results (seeing detailed discussion in Figure S1).

XPS Measurements. To investigate the possible changes of specific oxygen content, all the GO and rGO samples are tested by XPS experiments (Figure 2). The XPS spectra for the four samples can be well divided into four bands, peaking at 284.8, 286.9, 288, and 289.6 eV, corresponding to C–C, C–O, C=O, and O–C=O, respectively. The relative peak height ratios for sample 1 to sample 4 are 1:0.959:0.218:0.103, 1:0.982:0.176:0.111, 1:0.744:0.188:0.16, and 1:0.513:0.158:0.162, respectively. The resulting oxygen contents of four samples are 35.26%, 35.13%, 34.17%, and 29.64% from sample 1 to sample 4. The subsequently decreased oxygen content for each sample matches with the prediction that during the sample preparation procedure, longer reduction time, lower oxygen content. We can see that the oxygen content of sample 4 is the lowest, and the reducing of C–O is largest among the four samples. This change trend of the C–O peak height ratio in Figure 2 also implies that the remarkable reduction of the C–O groups could be one of the main reasons for the insulator–semiconductor–semimetal transitions of GO during the reduction treatment.

Selective Excitation Transient Absorption. Then, we use three pump lights (400, 500, and 600 nm, respectively) to excite the GO and rGO samples in broad-band femtosecond transient absorption spectroscopic experiments (Figure 3). Since the transient absorption spectra of sample 2 (slightly reduced GO) are very similar to that of sample 1 (as-prepared GO), it is not shown in Figure 3. For the sample 1 (GO with oxygen content of 35.26%, Figure 3a–c), it contains a relatively strong excited-state absorption signal (positive signal) compared to those of sample 3 (Figure 3d–f) and sample 4 (Figure 3g–i). And the ground-state bleaching peak signal (negative signal) becomes broader and broader from sample 1 to sample 4 under the same pump conditions (detailed discussions are presented below).

The excited-state absorption signal of GO can be attributed to the oxygen-containing functional groups, which is based on the model that sp^2 domains are surrounded by sp^3 -hybridized carbon atoms in GO and its reduced derivatives.^{24,27,28} So, the obtained transient spectral evolutions (positive signal part) of

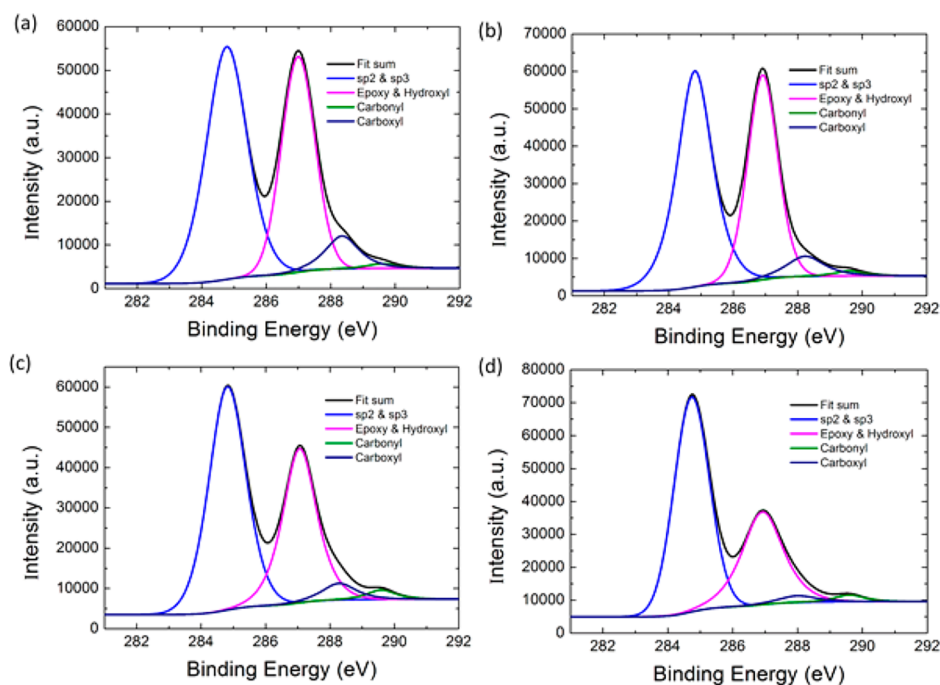


Figure 2. XPS spectra of GO and rGO with the reduction of oxygen content from (a)–(d) sample 1 to sample 4.

GO and rGO presented in Figure 3 are in agreement with the results of XPS (Figure 2). In addition, the relative intensities of the excited-state absorption signal (the ratio of the positive excited-state absorption signal to the negative ground-state bleaching signal) of sample 1 in 500 and 600 nm excitation experiments are weaker than that in the 400 nm excitation experiment. This is because the higher pump energy (i.e., 400 nm pump light) can mainly excite the oxygen-containing functional groups in sp^3 regions, which encircle a small amount of sp^2 clusters, while the relatively lower pump energy (i.e., 500 and 600 nm pump lights) mainly excites the quantum confined sp^2 domains (the size of those sp^2 domains should be larger than sp^2 clusters).^{24,28} Furthermore, we also observe that the normalized spectral shape of bleaching signal in sample 1 is not changed in the signal decay process (as shown in Figure S2a). This indicates the photogenerated carriers in each pump light do not transfer to larger sp^2 domains (insulator type); otherwise, the ground-state bleaching signals should be red shift as probe time increases.

However, for sample 3 (rGO with oxygen content of 34.17%, Figure 3d), we clearly observe this normalized ground-state bleaching signal red shifts as the probe time increases (Figure S2b). In addition, the red side parts of the ground-state bleaching peaks in the 500 nm (Figure 3e) and 600 nm (Figure 3f) excitation experiments are larger than their blue side parts. Especially, in the 600 nm excitation experiment, this red side part of the bleaching signal even begins to extend to 850 nm, accompanied by the disappeared positive excited-state absorption signal. This indicates that the larger size sp^2 domains have been occupied due to the instantaneous charge transfer from the smaller sp^2 domains excited by the pump light. That is a semiconductor-like behavior, which means the photoinduced carriers in smaller sp^2 clusters generated by high-energy photons absorbing can quickly relax into the lower energy sites assembled by larger sp^2 domains in vicinity of the original excited regions (so-called band gaps for semiconductor-type rGO; it is usually at around 500–600 nm,

corresponding to energy states from 2.07 to 2.48 eV). Considering there is only $\sim 1\%$ difference between the oxygen contents of sample 3 and sample 1 (or sample 2), it indicates the critical oxygen content for this insulator–semiconductor transition in GO and rGO samples.

When the oxygen content of rGO decreases as low as that in sample 4 (rGO with oxygen content of 29.64%), we can see new spectral phenomena in broad-band selective excitation transient absorption spectroscopic experiments. At the 400 nm excitation condition (Figure 3g), the positive excited-state absorption signal already disappeared, and it seems there is one negative bleaching peak located at 460 nm with a shoulder at 580 nm. As a result, the bleaching signal for sample 4 is the broadest. In the 500 nm (Figure 3h) and 600 nm (Figure 3i) excitation conditions, the bleaching signals are further red-shifted in comparison with the positions of pump lights and easily broadened to 850 nm. We propose that those transient spectroscopic results for sample 4 imply a semimetal-type behavior, which is different from that of semiconductor-type rGO (sample 3). The semimetal-like rGO can make photo-induced carriers populating on all possible exciton states at the initially excited moment.^{29,30} As a result, it will lead to a broad bleaching signal, as we observed in sample 4 in the UV–visible-near-infrared probe window, which is similar to the initial transient absorption spectra of CVD-grown graphene films (semimetal type).³⁰ It is worth noting that the semimetal-like rGO (sample 4) possesses the bleaching features of both semiconductor-type band gap of rGO (i.e., Figure 3g, under 400 nm excitation) and semimetal-type graphene (i.e., Figure 3h,i, under 500 and 600 nm excitations), depending on the excitation wavelength. This indicates a two-phase coexistence phenomenon, due to the nature of inhomogeneity of rGO. The normalized carrier dynamics for GO and rGO under 600 nm excitation experiments reflects that less oxygen content yields faster carrier relaxation (Figure 4), which is consistent with the observed insulator–semiconductor–semimetal transitions. The carrier dynamics of semiconductor-like (sample 3) and

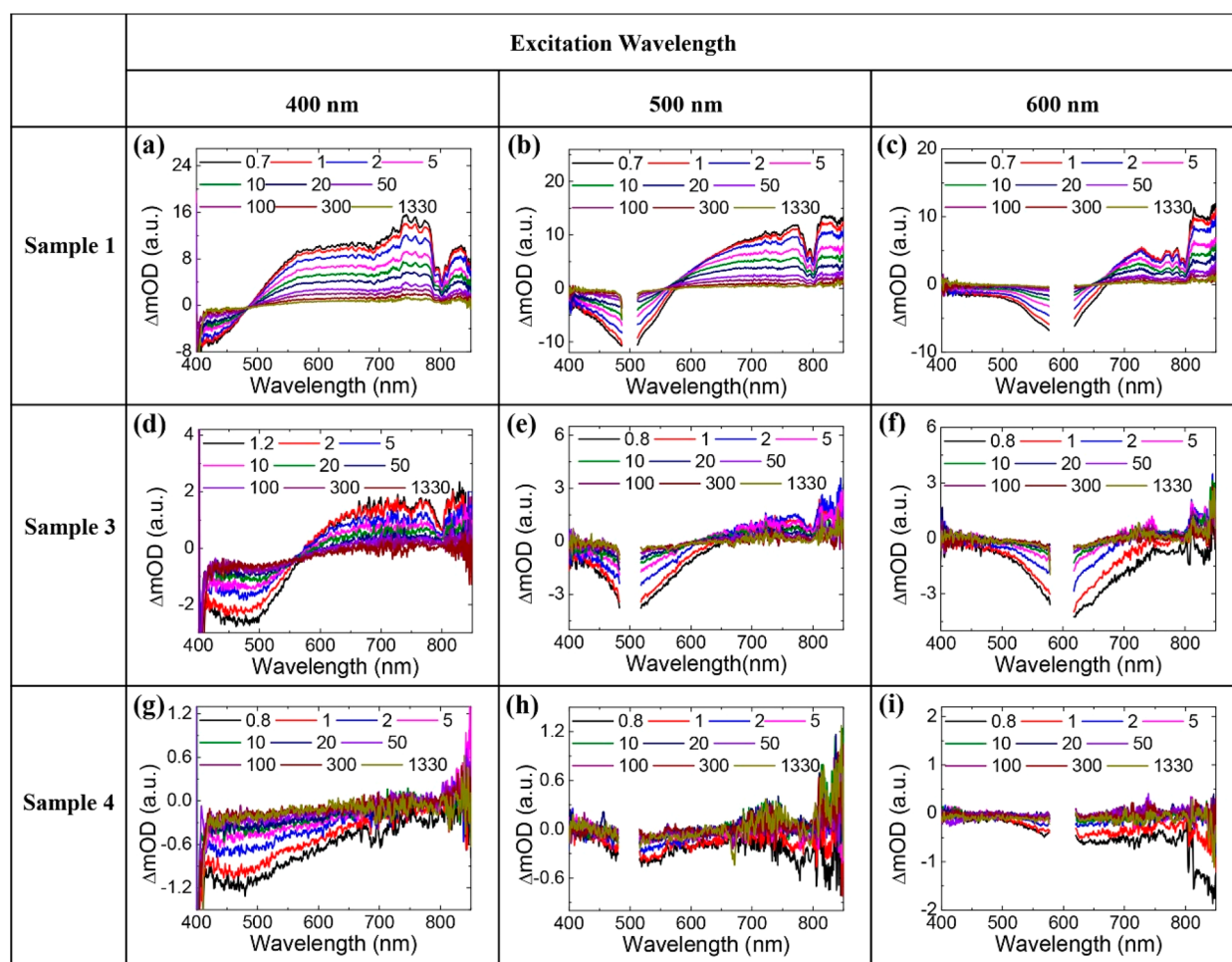


Figure 3. Transient absorption spectra of GO and rGO under different excitation wavelengths. (a)–(c) sample 1, (d)–(f) sample 3, and (g)–(i) sample 4. The selective excitation wavelength is at (a, d, g) 400 nm, (b, e, h) 500 nm, and (c, f, i) 600 nm, respectively. The picosecond unit is used in each panel. To rule out the influence of pump lights, the spectral ranges around 500 and 600 nm corresponding to pump lights are cut out. At the region near 800 nm, the disturbances in probe signals are from the limitation of supercontinuum white light.

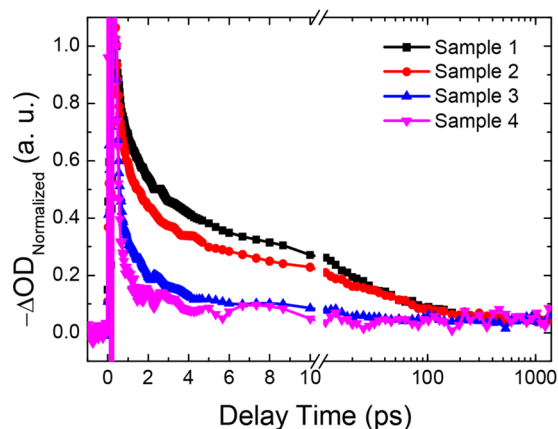


Figure 4. Normalized carrier dynamics probed at 570 nm for GO (sample 1) and rGO (sample 2 to sample 4) under 600 nm excitation experiments.

semimetal-like (sample 4) rGO obviously decays more quickly than insulator-like GO (sample 1) and rGO (sample 2), since for the former, the carrier transfer from small size sp^2 domains to larger size sp^2 domains is much easier than that in the latter.

Dual Roles of Semimetal-Like rGO. It is surprising that the initial semimetal feature occurs at a relatively high oxygen

content of $\sim 29\%$ for rGO. As a result, for pure semiconductor-like rGO, it only corresponds to a narrow range of oxygen content from $\sim 34\%$ to $\sim 29\%$. Instead, since the semimetal-like rGO possesses both roles of semiconductor and semimetal, it actually has a broader range of oxygen content, $< 29\%$. Thus, in previously reported rGO-based applications, most of them are related to the semimetal-like rGO. For example, when the oxygen content of rGO is between 29% and 20%, the semiconductor part of rGO is less, and the semimetal part of rGO becomes more and more. This dual role of semimetal-like rGO makes it achieve the capability of tunable multiresponses, which is the fundamental mechanism for the light-driven and humidity-responsive rGO actuators.^{31,32} When the oxygen content of rGO is less than 20%, its metallic properties are dominant, facilitating the fabrication of electrical-driven rGO-based devices, like micro-OLEDs operated on rGO electrodes³³ and rGO-based electrothermal actuators.³⁴

Insulator–Semiconductor–Semimetal Transitions. Finally, in order to visually understand the proposed transitions in GO and rGO, we have presented a schematic diagram shown in Figure 5. For insulator-like GO and rGO (oxygen content, $> 35\%$), due to the presence of high-density oxygen-containing functional groups around the sp^2 clusters, photo-induced electrons and holes are trapped in the sp^2 domains, which cannot be transferred. So, it exhibits the “insulation”

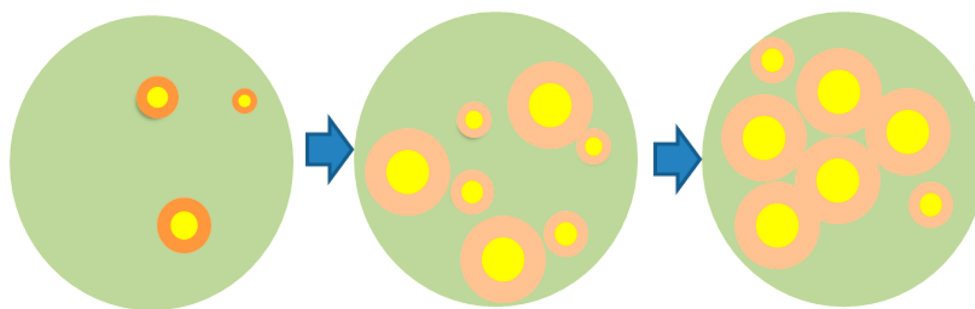


Figure 5. Schematic diagram of insulator (left)–semiconductor (middle)–semimetal (right) transitions for GO and rGO. The green area (so-called sp^3 matrix) is mainly covered by the oxygen-containing functional groups. Yellow areas are the small sp^2 clusters and large sp^2 domains. Orange areas are the peripheral structures with high sp^3/sp^2 carbon ratios around small sp^2 clusters (light orange areas mean the peripheral structures have relatively lower sp^3/sp^2 carbon ratio around large sp^2 domains).

property. For semiconductor-like rGO (oxygen content from $\sim 34\%$ to $\sim 29\%$), the reduction of the amount of oxygen-containing functional groups results in larger sp^2 domains generated near the relatively smaller sp^2 clusters. Thus, when the small sp^2 clusters absorb suitable photon energy, the photogenerated carriers can transfer from small sp^2 clusters to large sp^2 domains in the vicinity. As the oxygen content of rGO further decreases, it begins to be semimetal-like rGO (oxygen content, $< 29\%$). It means that in some parts of semimetal-like rGO, the sp^2 domains are almost connected to each other, because their boundaries consisting of relatively lower sp^3/sp^2 carbon ratio cannot strictly limit the photogenerated carrier transfer among those sp^2 domains. In this case, the rest of the semimetal-like rGO could be still semiconductor-like.

CONCLUSIONS

Through femtosecond selective excitation (at 400, 500, and 600 nm) transient absorption spectroscopic experiments and corresponding XPS results, we observe the transition processes in GO and rGO with different oxygen contents. We find that when the oxygen content of rGO is as low as $\sim 34\%$, it changes from insulator-like properties to semiconductor-like properties with a band gap in the range 2.07–2.48 eV; when the oxygen content of rGO is further decreased to $\sim 29\%$, the semimetal states in rGO initially occur. Those findings renew the knowledge that the most common form of rGO utilized in electrical applications is actually the semimetal-like rGO with dual roles, rather than pure semiconductor-like rGO. Our experimental results will be beneficial for understanding the photophysical properties of GO and rGO and related functional information for GO-based optoelectronic devices.

ASSOCIATED CONTENT

Supporting Information

The Supporting Information is available free of charge on the ACS Publications website at DOI: 10.1021/acs.jpcc.9b03926.

Discussion on the contributions of absorption and light scattering to the steady-state absorption spectrum of rGO; normalized bleaching signal evolution for sample 1 and sample 3 under 400 nm excitation conditions (PDF)

AUTHOR INFORMATION

Corresponding Authors

*Tel: + 81-431-8516-8281. Fax: + 81-431-8516-8270. E-mail: lei_wang@jlu.edu.cn (Lei Wang).

*Tel: + 81-431-8516-8281. Fax: + 81-431-8516-8270. E-mail: haiyu_wang@jlu.edu.cn (Hai-Yu Wang).

ORCID

Lei Wang: 0000-0003-4304-2887

Qi-Dai Chen: 0000-0002-0921-7973

Author Contributions

The manuscript was written through contributions of all authors. All authors have given approval to the final version of the manuscript.

Notes

The authors declare no competing financial interest.

ACKNOWLEDGMENTS

This work was supported by the National Key Research and Development Program of China and the National Natural Science Foundation of China (NSFC) under Grants 2017YFB1104300, 21773087, 21473077, 21603083, 61590930, and 61435005, as well as by the China Postdoctoral Science Foundation (2016M590259) and “the Fundamental Research Funds for the Central Universities”.

REFERENCES

- (1) Loh, K. P.; Bao, Q. L.; Eda, G.; Chhowalla, M. Graphene Oxide as a Chemically Tunable Platform for Optical Applications. *Nat. Chem.* **2010**, *2*, 1015–1024.
- (2) Chen, D.; Feng, H. B.; Li, J. H. Graphene Oxide: Preparation, Functionalization, and Electrochemical Applications. *Chem. Rev.* **2012**, *112*, 6027–6053.
- (3) Yeh, T. F.; Chen, S. J.; Yeh, C. S.; Teng, H. S. Tuning the Electronic Structure of Graphite Oxide Through Ammonia Treatment for Photocatalytic Generation of H_2 and O_2 from Water Splitting. *J. Phys. Chem. C* **2013**, *117*, 6516–6024.
- (4) Gan, T.; Hu, S. Electrochemical Sensors Based on Graphene Materials. *Microchim. Acta* **2011**, *175*, 1–19.
- (5) Kang, X.; Wang, J.; Wu, H.; Aksay, I. A.; Liu, J.; Lin, Y. H. Glucose Oxidase-Graphene-Chitosan Modified Electrode for Direct Electrochemistry and Glucose Sensing. *Biosens. Bioelectron.* **2009**, *25*, 901–905.
- (6) Si, Y.; Samulski, E. T. Synthesis of Water Soluble Graphene. *Nano Lett.* **2008**, *8*, 1679–1682.
- (7) Lee, D. W.; De Los Santos, V. L.; Seo, J. W.; Felix, L. L.; Bustamante, A.; Cole, J. M.; Barnes, C. H. W. The Structure of Graphite Oxide: Investigation of Its Surface Chemical Groups. *J. Phys. Chem. B* **2010**, *114*, 5723–5728.
- (8) Cai, W. W.; Piner, R. D.; Stadermann, F. J.; Park, S.; Shaibat, M. A.; Ishii, Y.; Yang, D. X.; Velamakanni, A.; An, S. J.; Stoller, M.; et al. Synthesis and Solid-State NMR Structural Characterization of ^{13}C -Labeled Graphite Oxide. *Science* **2008**, *321*, 1815–1817.

- (9) Bagri, A.; Mattevi, C.; Acik, M.; Chabal, Y. J.; Chhowalla, M.; Shenoy, V. B. Structural Evolution during the Reduction of Chemically Derived Graphene Oxide. *Nat. Chem.* **2010**, *2*, 581–587.
- (10) Acik, M.; Lee, G.; Mattevi, C.; Pirkle, A.; Wallace, R. M.; Chhowalla, M.; Cho, K.; Chabal, Y. The Role of Oxygen during Thermal Reduction of Graphene Oxide Studied by Infrared Absorption Spectroscopy. *J. Phys. Chem. C* **2011**, *115*, 19761–19781.
- (11) Gao, W.; Alemany, L. B.; Ci, L. J.; Ajayan, P. M. New Insights into the Structure and Reduction of Graphite Oxide. *Nat. Chem.* **2009**, *1*, 403–408.
- (12) Mattevi, C.; Eda, G.; Agnoli, S.; Miller, S.; Mkhoyan, K. A.; Celik, O.; Mastrogianni, D.; Granozzi, G.; Garfunkel, E.; Chhowalla, M. Evolution of Electrical, Chemical, and Structural Properties of Transparent and Conducting Chemically Derived Graphene Thin Films. *Adv. Funct. Mater.* **2009**, *19*, 2577–2583.
- (13) Akhavan, O.; Abdollahad, M.; Esfandiari, A.; Mohatashamifar, M. Photodegradation of Graphene Oxide Sheets by TiO₂ Nanoparticles After a Photocatalytic Reduction. *J. Phys. Chem. C* **2010**, *114*, 12955–12959.
- (14) Chen, X.; Jia, B. H.; Zhang, Y. N.; Gu, M. Exceeding the Limit of Plasmonic Light Trapping in Textured Screen-Printed Solar Cells Using Al Nanoparticles and Wrinkle-Like Graphene Sheets. *Light: Sci. Appl.* **2013**, *2*, No. e92.
- (15) Zhang, X. Y.; Sun, S. H.; Sun, X. J.; Zhao, Y. R.; Chen, L.; Yang, Y.; Lv, W.; Li, D. B. Plasma-Induced, Nitrogen-Doped Graphene-Based Aerogels for High-Performance Supercapacitors. *Light: Sci. Appl.* **2016**, *5*, No. e16130.
- (16) Yang, C.; Huang, Y. X.; Cheng, H. H.; Jiang, L.; Qu, L. T. Rollable, Stretchable, and Reconfigurable Graphene Hygroelectric Generators. *Adv. Mater.* **2019**, *31*, 1805705.
- (17) Ganguly, A.; Sharma, S.; Papakonstantinou, P.; Hamilton, J. Probing the Thermal Deoxygenation of Graphene Oxide Using High-Resolution in Situ X-Ray-Based Spectroscopies. *J. Phys. Chem. C* **2011**, *115*, 17009–17019.
- (18) Paredes, J. I.; Villar-Rodil, S.; Solis-Fernandez, P.; Martinez-Alonso, A.; Tascon, J. M. D. Atomic Force and Scanning Tunneling Microscopy Imaging of Graphene Nanosheets Derived From Graphite Oxide. *Langmuir* **2009**, *25*, 5957–5968.
- (19) Gómez-Navarro, C.; Meyer, J. C.; Sundaram, R. S.; Chuvilin, A.; Kurasch, S.; Burghard, M.; Kern, K.; Kaiser, U. Atomic Structure of Reduced Graphene Oxide. *Nano Lett.* **2010**, *10*, 1144–1148.
- (20) Kudin, K. N.; Ozbas, B.; Schniepp, H. C.; Prud'homme, R. K.; Aksay, I. A.; Car, R. Raman Spectra of Graphite Oxide and Functionalized Graphene Sheets. *Nano Lett.* **2008**, *8*, 36–41.
- (21) Jung, I.; Dikin, D. A.; Piner, R. D.; Ruoff, R. S. Tunable Electrical Conductivity of Individual Graphene Oxide Sheets Reduced at “Low” Temperatures. *Nano Lett.* **2008**, *8*, 4283–4287.
- (22) Kaiser, A. B.; Gomez-Navarro, C.; Sundaram, R. S.; Burghard, M.; Kern, K. Electrical Conduction Mechanism in Chemically Derived Graphene Monolayers. *Nano Lett.* **2009**, *9*, 1787–1792.
- (23) Eda, G.; Mattevi, C.; Yamaguchi, H.; Kim, H. K.; Chhowalla, M. Insulator to Semimetal Transition in Graphene Oxide. *J. Phys. Chem. C* **2009**, *113*, 15768–15771.
- (24) Wang, L.; Wang, H. Y.; Wang, Y.; Zhu, S. J.; Zhang, Y. L.; Zhang, J. H.; Chen, Q. D.; Han, W.; Xu, H. L.; Yang, B.; et al. Direct Observation of Quantum-Confined Graphene-Like States and Novel Hybrid States in Graphene Oxide by Transient Spectroscopy. *Adv. Mater.* **2013**, *25*, 6539–6545.
- (25) Wang, L.; Wang, Z.; Wang, H. Y.; Grinblat, G.; Huang, Y. L.; Wang, D.; Ye, X. H.; Li, X. B.; Bao, Q. L.; Wee, A. T. S.; et al. Slow Cooling and Efficient Extraction of C-exciton Hot Carriers in MoS₂ Monolayer. *Nat. Commun.* **2017**, *8*, 13906.
- (26) Chen, X.; Wang, Z.; Wang, L.; Wang, H. Y.; Yue, Y. Y.; Wang, H.; Wang, X. P.; Wee, A. T. S.; Qiu, C. W.; Sun, H. B. Investigating the Dynamics of Excitons in Monolayer WSe₂ Before and After Organic Super Acid Treatment. *Nanoscale* **2018**, *10*, 9346–9352.
- (27) Chien, C. T.; Li, S. S.; Lai, W. J.; Yeh, Y. C.; Chen, H. A.; Chen, I. S.; Chen, L. C.; Chen, K. H.; Nemoto, T.; Isoda, S.; et al. Tunable Photoluminescence from Graphene Oxide. *Angew. Chem., Int. Ed.* **2012**, *51*, 6662–6666.
- (28) Zhang, Q.; Zheng, H. J.; Geng, Z. G.; Jiang, S. L.; Ge, J.; Fan, K. L.; Duan, S.; Chen, Y.; Wang, X. P.; Luo, Y. The Realistic Domain Structure of As-Synthesized Graphene Oxide from Ultrafast Spectroscopy. *J. Am. Chem. Soc.* **2013**, *135*, 12468–12474.
- (29) Limmer, T.; Feldmann, J.; Da Como, E. Carrier Lifetime in Exfoliated Few-Layer Graphene Determined From Intersubband Optical Transitions. *Phys. Rev. Lett.* **2013**, *110*, 217406.
- (30) Shang, J. Z.; Yu, T.; Lin, J. Y.; Gurzadyan, G. G. Ultrafast Electron-Optical Phonon Scattering and Quasiparticle Lifetime in CVD-Grown Graphene. *ACS Nano* **2011**, *5*, 3278–3283.
- (31) Han, D. D.; Liu, Y. Q.; Ma, J. N.; Mao, J. W.; Chen, Z. D.; Zhang, Y. L.; Sun, H. B. Biomimetic Graphene Actuators Enabled by Multiresponse Graphene Oxide Paper with Pretailored Reduction Gradient. *Adv. Mater. Technol.* **2018**, *3*, 1800258.
- (32) Han, D. D.; Zhang, Y. L.; Liu, Y.; Liu, Y. Q.; Jiang, H. B.; Han, B.; Fu, X. Y.; Ding, H.; Xu, H. L.; Sun, H. B. Bioinspired Graphene Actuators Prepared by Unilateral UV Irradiation of Graphene Oxide Papers. *Adv. Funct. Mater.* **2015**, *25*, 4548–4557.
- (33) Bi, Y. G.; Feng, J.; Li, Y. F.; Zhang, Y. L.; Liu, Y. S.; Chen, L.; Liu, Y. F.; Guo, L.; Wei, S.; Sun, H. B. Arbitrary Shape Designable Microscale Organic Light-Emitting Devices by Using Femtosecond Laser Reduced Graphene Oxide as a Patterned Electrode. *ACS Photonics* **2014**, *1*, 690–695.
- (34) Zhu, L.; Gao, Y. Y.; Han, B.; Zhang, Y. L.; Sun, H. B. Laser Fabrication of Graphene-Based Electrothermal Actuators Enabling Predictable Deformation. *Opt. Lett.* **2019**, *44*, 1363–1366.